Journal of Photochemistry and Photobiology A: Chemistry 231 (2012) 9–18

Contents lists available at SciVerse ScienceDirect

Journal of Photochemistry and Photobiology A: Chemistry

journal homepage: www.elsevier.com/locate/jphotochem

Rice grain-shaped TiO_2–CNT composite—A functional material with a novel morphology for dye-sensitized solar cells

Zhu Peining[a], A. Sreekumaran Nair[b,*], Yang Shengyuan[c], Peng Shengjie[d], Naveen Kumar Elumalai[a], Seeram Ramakrishna[a,b,**]

[a] Department of Mechanical Engineering, National University of Singapore, Singapore 117574, Singapore
[b] Healthcare and Energy Materials Laboratory, Nanoscience and Nanotechnology Initiative, National University of Singapore, Singapore 117581, Singapore
[c] NUS Graduate School for Integrative Sciences and Engineering, National University of Singapore, Singapore 117456, Singapore
[d] School of Materials Science and Engineering, Nanyang Technological University, Singapore 639798, Singapore

ARTICLE INFO

Article history:
Received 28 September 2011
Received in revised form
22 December 2011
Accepted 7 January 2012
Available online 16 January 2012

Keywords:
Titanium dioxide
Carbon nanotubes
Composite materials
Hybrid materials
Photovoltaic devices

ABSTRACT

Titanium dioxide-multiwalled carbon nanotube (denoted as TiO_2–CNT) nanocomposites with a novel rice-grains nanostructure are synthesized by electrospinning and subsequent high temperature sintering. The rice grain-shaped TiO_2 is single crystalline with a large surface area and the single crystallinity is retained in the TiO_2–CNT composite as well. At very low CNT loadings (0.1–0.3 wt% of TiO_2), the rice grain shape remains unchanged while at high CNT concentrations (8 wt%), the morphology distorts with CNTs sticking out of the rice-grain shape. The optimum concentration of CNTs in the TiO_2 matrix for best performance in dye-sensitized solar cells (DSCs) is found to be 0.2 wt%, which shows a 32% enhancement in the energy conversion efficiency. The electrochemical impedance spectroscopy (EIS) and the incident photon-to-electron conversion efficiency (IPCE) measurements show that the charge transfer and collection are improved by the incorporation of CNTs into the rice grain-shaped TiO_2 network. We believe that this facile one-pot method for the synthesis of the rice-grain shaped TiO_2–CNT composites with high surface area and single crystallinity offers an attractive means for the mass-scale fabrication of the nanostructures for DSCs since electrospinning is a simple, cost-effective and scalable means for the commercial scale fabrication of one-dimensional nanostructures.

1. Introduction

Since the first report by Grätzel in 1991 [1], dye-sensitized solar cells (DSCs) have gained considerable attention as the next generation solar cells because of their advantages such as simple non-vacuum fabrication, high efficiency to the tune of 11% [2], ease of large-scale production [2] and benefits comparable to that of amorphous silicon (Si) solar cells [3]. As the most extensively used semiconductor in the application of DSCs, many morphologies and fabrication steps for TiO_2 have been studied in the past two decades for improving the device performance. Several new steps in DSC fabrication have been introduced such as incorporation of a compact hole-blocking layer of TiO_2 on FTO (fluorine-doped tin oxide) [4], an additional scattering layer made of ~400 nm TiO_2 particles on top of the active TiO_2 layer [5], $TiCl_4$ treatment [6], and sensitization of TiO_2 with a mixture of dyes having different spectral responses [7]. Doping of TiO_2 with non-metals (e.g. nitrogen and silica) has also been explored [8,9].

However, the transport of photo-injected electrons across the TiO_2 network is the major limiting factor in attaining higher overall conversion efficiencies in DSCs. It is well known that the transport of photo-injected electrons across the TiO_2 network occurs by diffusion and is strongly hindered by trapping and de-trapping events at grain boundaries and particle surfaces. The random path of photo-injected electrons in the TiO_2 network increases the probability of their recombination with oxidized dye species or the tri-iodide electrolyte and hence a rapid transport of the electrons across the TiO_2 network is desired for faster collection [10]. Therefore, one dimensional (1-D) TiO_2 nanostructures have attracted the attention of scientists owing to their high surface area for dye absorption [11], enhancing the light harvesting efficiency by scattering more light at the red part of the solar spectrum [12], high intrinsic electron mobility [13], and semi-directed charge transport [14]. The use of 1-D nanostructures is supposed to shorten the electron transport pathways and enhance the accessibility of electrodes to the hole-transporting materials [15]. Several research

* Corresponding author. Tel.: +65 6516 6593; fax: +65 6773 0339.
** Corresponding author at: Healthcare and Energy Materials Laboratory, Nanoscience and Nanotechnology Initiative, National University of Singapore, Singapore 117581, Singapore.
E-mail addresses: nniansn@nus.edu.sg (A.S. Nair), seeram@nus.edu.sg (S. Ramakrishna).

1010-6030/$ – see front matter © 2012 Elsevier B.V. All rights reserved.
doi:10.1016/j.jphotochem.2012.01.002

efforts have happened/are ongoing in this direction, especially the design of one-dimensional oxide nanostructures such as nanofibers (random and aligned), nanowires, vertically oriented nanotubes and nanorods [16–18]. The transport and recombination studies on the oriented nanotubes showed an enhanced suppression of the recombination, while maintaining a relatively smooth charge transport [19].

Recently, incorporation of CNTs into TiO_2 matrix has attracted the attention of scientists as a possible means to increase the efficiency of the DSC devices in view of the superior electronic properties and ease of surface functionalization of the former [20,21]. It is demonstrated that incorporation of CNTs into the TiO_2 matrix would enhance the conductivity of the TiO_2 aggregates, which would facilitate faster electron transport across the TiO_2 network thus minimizing charge recombination. TiO_2–CNT composites have been used in DSCs by several groups [10,20–26]. Sawatsuk et al. [24] achieved an efficiency enhancement of ~60% by the incorporation of non-functionalized CNTs into the TiO_2 particles by ultrasonication (however, no *I–V* graph has been shown in the manuscript). Muduli et al. [23] observed that the efficiency of DSCs could be increased by 50% when a few mg of CNTs have been incorporated into the P-25 TiO_2 particles by hydrothermal treatment. Enhancements to much lower levels have been reported in TiO_2-coated CNTs (by sol–gel method) by Kamat et al. [10,22], Lee et al. [20], Yen et al. [25], and Jang et al. [26], respectively. TiO_2–CNT nanocomposites could be fabricated through methods such as blending [27], chemical vapor deposition [28], electrospinning [29–31], physical vapor deposition [32], sol–gel [33] and hydrothermal [23].

Recently, we have found a methodology to fabricate uniformly distributed, rice grain-shaped, single crystalline TiO_2 nano/mesostructures of high surface area by electrospinning [34]. The rice grain-shaped TiO_2 showed superior activity than the commercially available P-25 TiO_2 in photovoltaics and photocatalysis [34,35]. The methodology was extended further in fabricating rice grain-shaped TiO_2–CNT nanocomposites with superior photocatalytic and Li-ion battery properties [36,37]. In the present work, the electrospun TiO_2-MWCNT (denoted hereafter as TiO_2–CNT) nanocomposites with various wt% of CNTs were employed in the application of DSCs as photoanodes. The composite was structurally characterized by spectroscopy and microscopy. Photovoltaic characteristics were analyzed by current–voltage (*I–V*) and incident photon-to-current conversion efficiency (IPCE) measurements. Charge transport through the TiO_2–CNT network was analyzed by electrochemical impedance spectroscopy (EIS). Systematic studies with devices having various amounts of CNTs incorporated into the TiO_2 network showed a 32% enhancement in the efficiency of DSCs when the CNT concentration was 0.2 wt% (in comparison to the amount of TiO_2). IPCE and EIS revealed insights into the enhanced transfer of the photoexcited electrons across the TiO_2 network and faster collection at the FTO. We believe that the simple fabrication of high performance TiO_2–CNT nanocomposite with the interesting morphology of rice grains by electrospinning could be widely employed in DSC applications, photocatalysis, self-cleaning membranes, etc.

2. Experimental

2.1. Materials

Titanium (IV) isopropoxide (TIP, 97%), polyvinyl acetate (PVAc, Mn = 500,000), *N*,*N*-dimethyl acetamide (DMAc, 99.8%), titanium(IV) chloride ($TiCl_4$, 99%), chloroplatinic acid hexahydrate ($H_2PtCl_4{\cdot}6H_2O$), isopropyl alcohol, lithium iodide, iodine, 4-tert-butylpyridine, 1-propyl 2,3-dimethyl imidazolium iodide, acetonitrile, and tert-butanol were from Aldrich (Steinheim, Germany) and used as received. Multiwalled carbon nanotubes (CNTs, purity > 98%, outer diameter between 10 and 20 nm and length between 1 and 2 μm) were purchased from Shenzhen Nanotech Port Co., Ltd. (Shenzhen, China). Acetic acid (99.7%) was from LAB-SCAN Analytical Sciences, Thailand. Methanol (CHROMASOLV, Aldrich), ethanol (absolute, Fischer scientific, Leicestershire, UK) and acetone (AR grade, Fisher Scientific, UK) were used as received. Fluorine-doped tin oxide (FTO, 1.5 cm × 1 cm, sheet resistance < 25 Ω/□) was from Asahi Glass, Japan. N3 dye ((cis-bis(4,4′-dicarboxy-2,2′-bipyridine)dithiocyanato ruthenium(II)) was purchased from Solaronix (Switzerland) and used as received. The FTO plates were cleaned in water, acetone and ethanol successively and dried at 80 °C in an oven. Millipore water was used in all experiments.

2.2. Rice grain-shaped TiO_2–CNT composites by electrospinning

The electrospinning solution was prepared from PVAc, DMAc, acetic acid, TIP and —COOH functionalized CNTs using a typical procedure previously reported by us [36]. Briefly, a few milligrams of the —COOH functionalized CNTs were dispersed in 10 mL DMAc by sonication for 3 h. The PVAc (1.2 g) was then added into the solution with stirring. After stirring for 15 min, 2 mL of glacial acetic and 1 mL of TIP, respectively, were added. The solution was kept under stirring for 12 h when the dark viscous solution became homogeneous. The solution was then subjected to electrospinning using a commercial machine (NANON, MECC Japan) with an applied voltage of 25 kV, working distance of 14 cm and a flow rate of 1.0 mL/h. The humidity level inside the electrospinning chamber was maintained around 50%. The electrospun fibers were collected on an aluminum foil which was wrapped around a rotating drum. The deposited fibers were removed in the form of a freestanding sheet and were sintered at 450 °C for 3 h with a ramping rate of 2 °C/min to get the rice grain-shaped composites. The amount of CNTs in the electrospinning solution was adjusted in such a manner to get 0.1, 0.2, and 0.3 wt% against TiO_2. Electrospinning was also done without CNTs for a comparison of the results with the bare rice grain-shaped TiO_2.

2.3. Fabrication of dye-sensitized solar cells (DSCs)

Clean (cleaned using water, acetone and ethanol successively and dried in an oven at 80 °C) FTO plates were treated with 50 mM $TiCl_4$ aqueous solution at 70 °C for 30 min, followed by twice screen-printing and one time doctor-blading of the TiO_2 (rice grain-shaped) paste on an area of ~0.25 cm^2. The paste was prepared by dispersing 100 mg rice grain-shaped TiO_2 into 100 μL polyester with 12 h sonication [38]. The film was heated at 450 °C in air for 30 min, treated with $TiCl_4$ solution and sintered again at 450 °C for 30 min. The TiO_2 electrodes were immersed in a 1:1 volume mixture of acetonitrile and tert-butanol solution of a ruthenium-based dye [$RuL_2(NCS)_2{\cdot}2H_2O$; L = 2,2′-bipyridyl-4,4′-dicarboxylic acid (0.5 mM, N3 Solaronix)] for overnight, washed with acetonitrile and dried in vacuum. The counter electrode was prepared by spin-coating H_2PtCl_4 (50 mM in isopropyl alcohol) on an FTO substrate and sintered at 390 °C in air for 30 min. Acetonitrile containing 0.1 M lithium iodide, 0.03 M iodine, 0.5 M 4-tert-butylpyridine, and 0.6 M 1-propyl 2,3-dimethyl imidazolium iodide was used as the electrolyte. Cell fabrication was completed by firmly clamping the two electrodes with an adhesive tape (45 μm) as the spacer film.

2.4. Characterization and measurements

The morphology of the as-spun fibers and the sintered nanostructures was investigated by scanning electron microscopy (SEM)

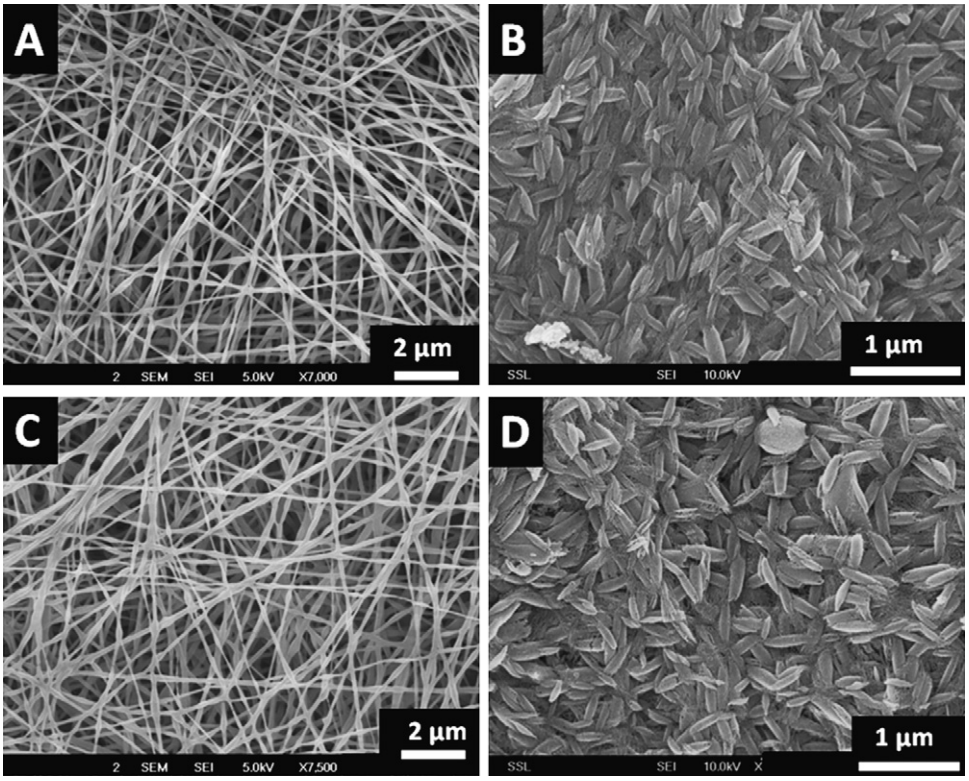

Fig. 1. SEM images of the as-spun TiO_2–CNT (0.2 wt%)–PVAc (A) and TiO_2–PVAc nanofibers (C). The sintered TiO_2–CNT nanocomposite and TiO_2 are shown (B) and (D), respectively, revealing the rice grain-shaped morphology.

(Quanta 200 FEG operated at 5–15 kV and JEOL JSM-6701F operated at 5–15 kV, respectively). The fine structure was investigated by transmission electron microscopy (TEM, JEOL 3010, operated at 300 kV). The XRD patterns and Raman spectra were recorded using a Siemens D5005 X-ray diffractometer employing Ni-filtered CuKα radiation and a Dilor model OMARS 89-Z24 microprobe spectrometer, using an Ar^+ ion laser at 514.5 nm wavelength, respectively. UV–vis spectra were measured using a Shimadzu UV-3600 UV-Vis-NIR spectrophotometer after ultrasonically dispersing the materials in methanol and infrared spectra were acquired using a NEXUS 670 spectrometer after dispersing the materials in a KBr matrix. The BET measurement was carried out using a NOVA 4200E Surface Area and Pore Size Analyzer (Quantachrome, USA). X-ray photoelectron spectroscopy (XPS) was performed with an ESCALab220i-XL electron spectrometer from VG Scientific. Monochromatic Al Kα X-ray ($h\nu$ = 1486.6 eV) was employed for analysis with an incident angle of 30° with respect to surface normal. Photoelectrons were collected at a take-off angle of 50° with respect to surface normal. The analysis area was approximately 400 μm in diameter while the maximum analysis depth lies in the range of 4–10 nm. Survey spectra and high-resolution spectra were acquired for surface composition analysis and for chemical state identification, respectively. Charge compensation was performed by means of low energy electron flooding and further correction was made based on adventitious C1 s at 285.0 eV using the manufacturer's standard software. The photocurrent–voltage (*I–V*) curves and the electrochemical impedance spectra (EIS) were measured by XES-151 S solar simulator (San-Ei, Japan) under AM1.5 G condition and an Autolab PGSTAT30 integrated with a potentiostat, respectively. EIS spectra of DSCs were measured at a bias voltage of 0.67 V under dark. Incident photon-to-electron conversion efficiency (IPCE) was measured using an IPCE evaluation system for dye-sensitized solar cells (Bunkoh-Keiki Co. Ltd., CEP-2000).

3. Results and discussion

3.1. Morphological and structural characterization

Fig. 1A and C shows the smooth, continuous and randomly oriented as-spun fibers of TiO_2–CNT (0.2 wt%)–PVAc and TiO_2–PVAc composites, respectively, obtained by electrospinning. The average diameter of the as-spun fibers was ~200 nm. Fig. 1B and D shows uniformly distributed rice grain-shaped nanocomposites of TiO_2–CNTs and TiO_2 obtained from the as-spun nanofibers by sintering at 450 °C for 3 h. Sintering results in near collapse of the continuous fiber morphology with the concomitant appearance of the excellently interconnected rice grain-shaped TiO_2 [34]. It has already been confirmed that the rice grain-like morphology resulted due to the microscale phase separation between TiO_2 and the PVAc (owing to the poor solubility of TiO_2 in the latter) during the solvent evaporation stage in the sintering process [34,35]. Evaporation of the polymer during the sintering process gave high porosity to the rice grain-like composites (see BET results below) and some of them were hollow as well. The average dimensions of the sintered nanostructures were 450 nm in length and 150 nm in diameter. It must be noted that the rice grain morphology was not because of the incorporation of CNTs into the TiO_2 network [35]. The excellent connectivity between the rice grain-like nanostructures could be beneficial in improving the electron transfer of photoinjected electrons in the TiO_2 network compared to the spherical particles [34,35]. It is known that for slightly elongated particles, the number of contacts per particle (within a region of diameter equal to twice the shortest thickness of the particle) is greater than for spherical particles as long as the aspect ratio is less than ~20 [39] (the aspect ratio in the present case is ~3). The 1D nature of elongated particles has a greater effect for particles of greater elongation, packing and contact effects are only greatest for slightly elongated particles [40] (such as the rice grain-shaped structures).

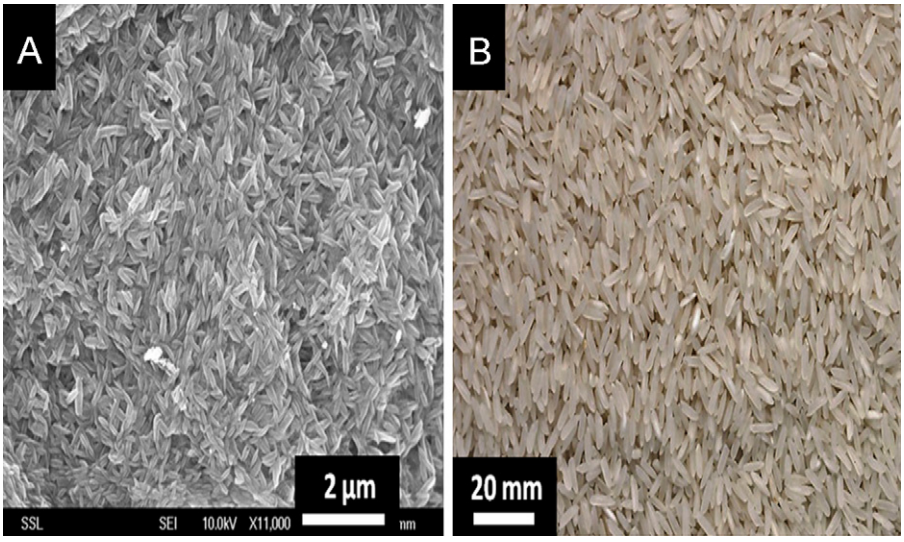

Fig. 2. A comparison of the shapes of TiO_2–CNT (0.2 wt%) composites (A) with that of genuine rice grains (B).

Due to the evaporation of polymer during the high temperature sintering process, the rice grain nanostructures were porous with a high surface area of ~62 m^2/g for the composite (with 0.2 wt% of CNTs) and ~60 m^2/g for the TiO_2. The slightly higher surface area of the composite could be due to the presence of small amounts of the CNTs as the latter is known to have extremely high surface areas [41]. For the intuitive understanding of the nomination of rice grain morphology, a comparison of the shapes of TiO_2–CNT nanostructures with that of genuine rice grains is provided in Fig. 2

The morphologies were further investigated by HR-TEM. Fig. 3A shows a resolved SEM image of the rice grains-like TiO_2–CNT (0.2 wt%) composite nanostructures and Fig. 3B shows a high-resolution TEM image of a single nanostructure. Images A and B in Fig. 4 show the respective images of the rice grain-shaped TiO_2

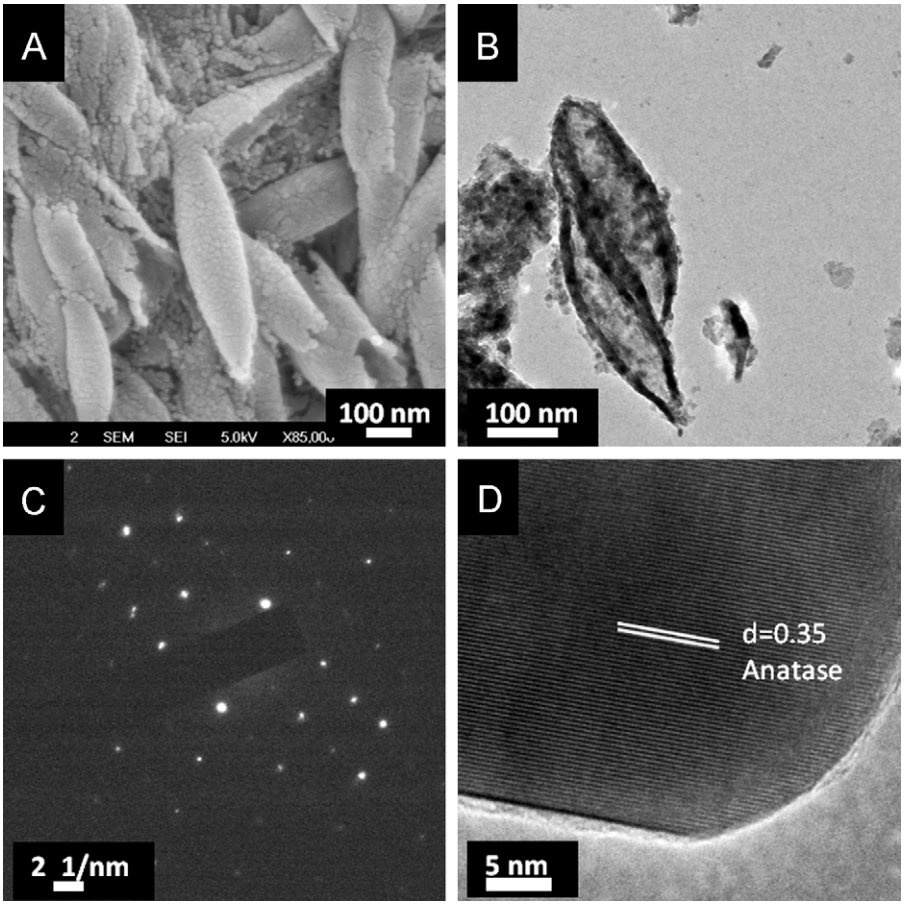

Fig. 3. SEM image (A), TEM image (B), SAED pattern (C), and lattice-resolved image (D) of TiO_2–CNT (0.2 wt%) nanocomposite.

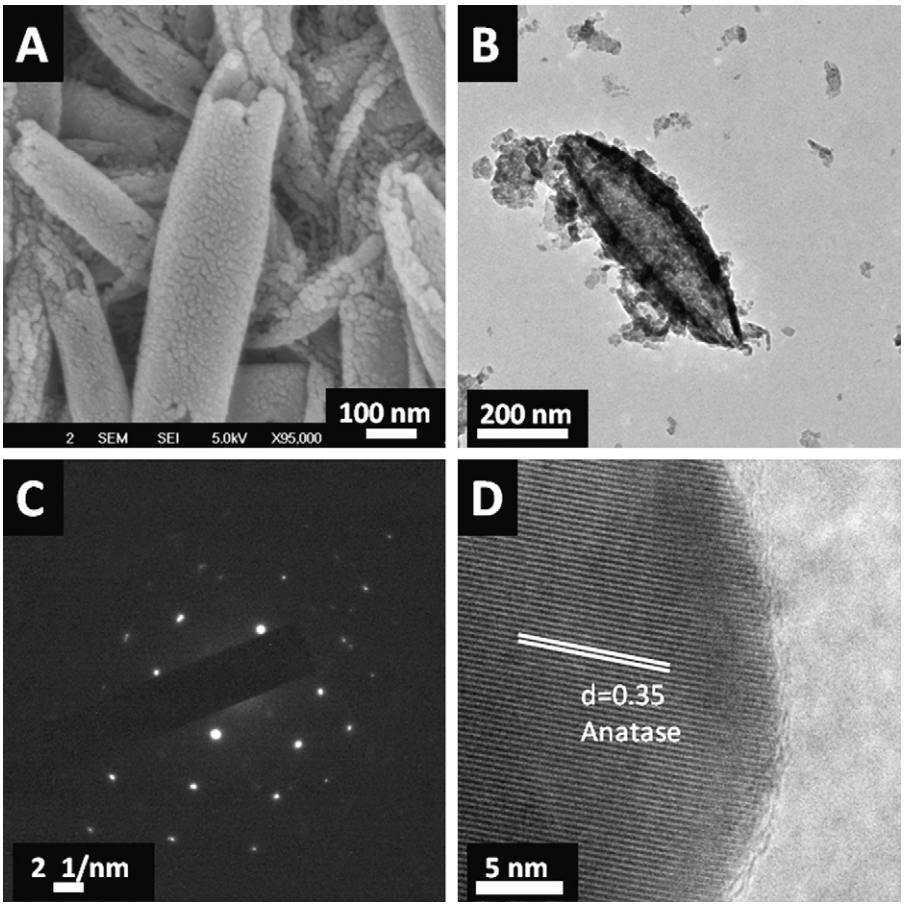

Fig. 4. SEM image (A), TEM image (B), SAED pattern (C), and lattice-resolved image (D) of TiO_2 rice grain nanostructure.

(when the electrospinning was done in the absence of CNTs). It was found that when the CNTs loadings in TiO_2 were low (between 0.1 and 0.3 wt%) the rice grain morphology was retained for the TiO_2–CNT composite. High-resolution images indicate that both TiO_2 and TiO_2–CNT nanostructures were made of spherical particles with diameter between 15 and 20 nm. Figs. 3C and 4C, respectively, show selected area electron diffraction (SAED) patterns of the nanocomposite and the TiO_2, indicating the single crystallinity of the TiO_2 in both. In coincident with the SAED pattern, the lattice-resolved images showed a perfect 0.35 nm lattice spacing corresponding to the anatase structure of TiO_2 (Figs. 3D and 4D, respectively). For low loadings of CNTs (0.1–0.3 wt%), no CNTs were visible even in high-magnification TEM images. However, at high CNT loadings (8 wt%), the CNTs were seen sticking out of the composite with a visible destruction of the rice grain-like morphology (SEM and TEM images in Fig. 5).

Fig. 6 shows the XRD patterns of TiO_2–CNT (0.2 wt%) nanocomposite and the TiO_2 nanostructures. As indicated by the SAED and the lattice-resolved images, the XRD patterns also revealed the presence of single-crystalline anatase TiO_2. The peaks in the pattern at 25.28 (1 0 1), 37.80 (0 0 4), 48.18 (2 0 0), and 54.09 (1 0 5) clearly represent the anatase phase of TiO_2 (PCPDFWIN # 211 272).

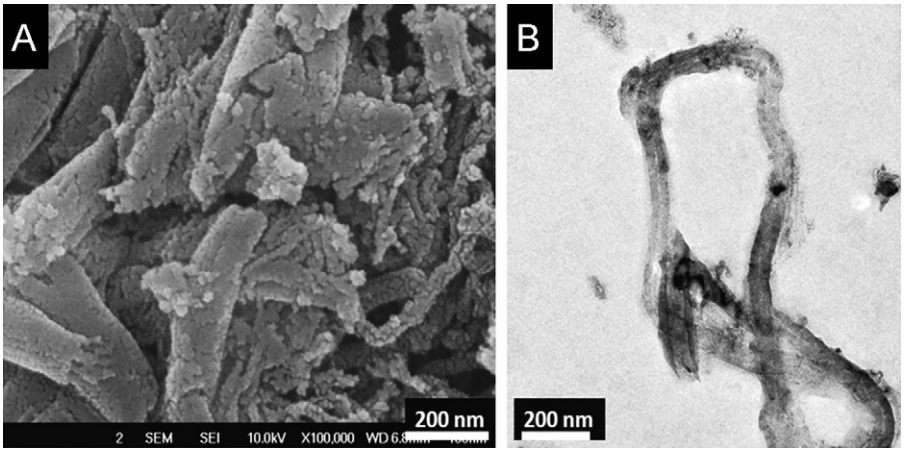

Fig. 5. SEM (A) and TEM (B) image, respectively, of TiO_2–CNT nanocomposite with high CNT content (8 wt%).

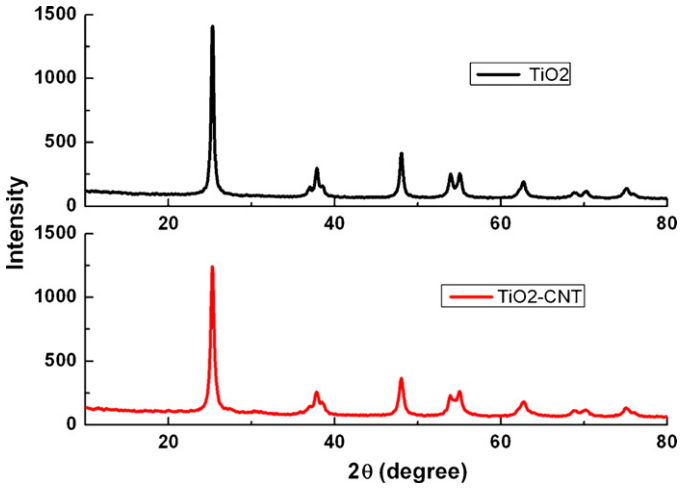

Fig. 6. XRD patterns of TiO_2 and TiO_2–CNT (0.2 wt%) nanocomposite.

The peaks corresponding to CNTs were not obvious in the XRD spectrum of the composites and is primarily because of two reasons: (a) overlap of [0 0 2] reflection of the CNTs at 26.4° [42] with the [1 0 1] reflection of anatase at $2\theta = 25.3°$ [23], (b) low intensity of the CNTs resulted from its low concentration compared to that of TiO_2 (0.2 wt% against TiO_2). A comparison of the UV–vis spectra (Supporting Information, SI-1) showed a shift of the absorption onset from UV (for TiO_2) to the visible region (for TiO_2–CNT) [36]. A comparison of the Raman spectra (SI-2) of the functionalized CNTs and the TiO_2–CNT showed lowering of the D/G ratio implying the robustness of CNTs in the composites [36]. The fabrication of the composite involves sintering at 450 °C for ~3 h and during this process, the disordered amorphous carbon (responsible for the D band in Raman spectrum) generated out of the acid-assisted functionalization gets burned-off, resulting in a more fraction of the ordered graphitic carbon (responsible for G band in the Raman spectrum) [36]. Raman spectrum also showed signatures of —COOH functionalized CNTs and their incorporation into the TiO_2 network [36]. Detailed characterization of the TiO_2–CNT nanocomposites have been done before using spectroscopies [36] and hence are not repeated in this paper. However, XPS spectra are presented as an obvious proof for the inclusion of CNTs into the TiO_2 matrix.

The XPS survey spectrum of the rice grain-shaped TiO_2 and TiO_2–CNT (0.3 wt%) composites are shown in Fig. 7A and B, respectively. The elemental composition is assigned in the spectra itself. While the C1 s peak was negligible in the case of TiO_2 (which indicates that there was no carbon related impurities left in TiO_2 due to polymer degradation), a prominent one can be seen in the case of the composite (marked with dotted circles). As both the samples were sintered under similar conditions, it can be concluded that the C1 s peak in TiO_2–CNT composites came directly from the CNTs and not as a result of impurity from the polymer decomposition process. Fig. 7C and D shows the high-resolution XPS spectra of Ti 2P of TiO_2 and the composite, respectively. The binding energies of Ti $2P_{3/2}$ and Ti $2P_{½}$ in bare TiO_2 were centered at 459.40 eV and 465.16 eV, respectively, corresponding to a spin–orbit coupling of 5.76 eV [43]. However, the same for TiO_2–CNT was slightly upshifted to 459.44 and 465.22 eV, respectively (minor differences less than 0.1 eV), which implies that the Ti in the TiO_2–CNT composites is in a slightly different chemical environment than that in TiO_2, indicating the chemical interaction between TiO_2 and the CNTs (that is primarily between the surface —OH groups of the TiO_2 and the —COOH groups of the functionalized CNTs) [44]. In the high-resolution spectrum of C 1 s (Fig. 7E), the main peak at 284.7 eV could be assigned to C—C and C=C bonds. The broad peak ranging from 284 eV to 292 eV was deconvoluted into three other peaks at 286.7 eV, 287.6 eV, and 288.2 eV, respectively [43,44]. The minor peaks from 286 to 289 eV could be due to the presence of oxidized components from the CNTs. Fig. 7F shows the high-resolution XPS spectrum of the O 1 s peak of the composite. The spectrum can also be deconvoluted into four peaks. The main peak at 530.5 eV could be ascribed to the O 1 s of TiO_2. The minor peaks at 532.3, 532.7 and 533.1 eV, respectively, could be due to the presence of undissociated H_2O molecules/—OH groups on TiO_2 surfaces [43,45]. Thus the XPS data indicate the oxidation of CNTs and their successful incorporation into the TiO_2 network.

3.2. Photocurrent–voltage (I–V) characteristics

In order to study the DSC performance of the rice grain-shaped TiO_2 nanostructure as well as the effect of incorporation of the CNTs into them, a series of DSCs were fabricated with the rice grain-shaped TiO_2 nanostructures and the TiO_2–CNT composites with different CNT concentrations as the electrodes. The thickness of the

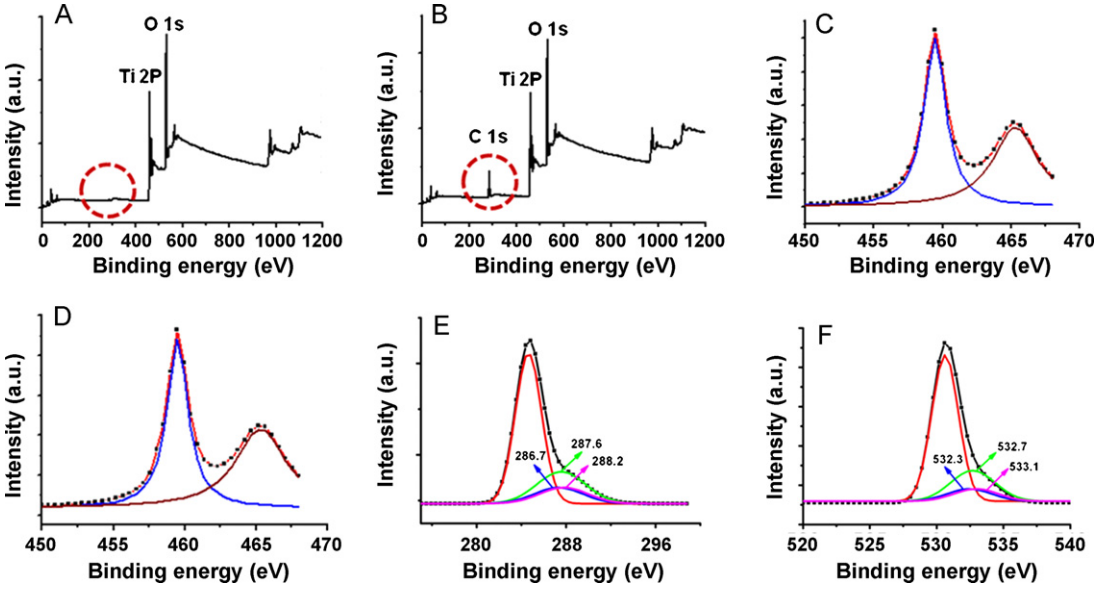

Fig. 7. XPS spectra of TiO_2 (A) and TiO_2–CNT (0.3 wt%) (B); and high-resolution XPS spectra of Ti 2p peak of TiO_2 (C) and TiO_2–CNT (D), C 1 s (E) and O 1 s (F) of TiO_2–CNT.

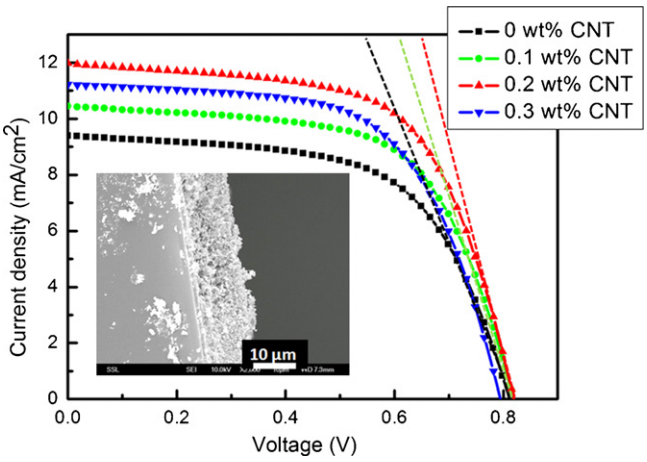

Fig. 8. *I–V* characteristics for CNTs-incorporated TiO_2 electrode in DSCs and cross-sectional SEM image showing the thickness of the electrodes (inset image).

electrodes was maintained at 11 μm for all the electrodes (see the inset of Fig. 8) as this was found to be the ideal thickness for DSCs with the materials [35,38].

The *I–V* characteristics of the different electrodes are presented in Fig. 8 and the results are summarized in Table 1. From the results, we can see that when the concentration of CNTs was increased from 0 to 0.2 wt%, the efficiency of the DSCs increased from 4.63% to 6.12%, with the short-circuit photocurrent density (J_{sc}) enhanced from 9.40 mA/cm^2 to 11.98 mA/cm^2, the open-circuit photovoltage (V_{oc}) increased from 0.815 V to 0.82 V, and the fill factor (FF) improved from 0.60 to 0.62. The increase in efficiency was primarily due to increase in J_{sc} as the increases in V_{oc} and FF were marginal. As an increase in J_{sc} is usually attributed to increase in dye-loading, the number of dye molecules present in the two electrodes were estimated by desorbing them using 0.02 M NaOH solution (50% (v/v) in water–ethanol mixture). The number of dye molecules present in TiO_2 electrodes was quantified (from the UV–vis spectra of the desorbed dyes given in Fig. 9A) to 1.61×10^{-7} mol/cm^2 and that on the TiO_2–CNT to 1.41×10^{-7} mol/cm^2. Thus it is obvious that the robust increase in J_{sc} from 9.4 mA/cm^2 to11.98 mA/cm^2 and hence the increase in efficiency was not due to an increase in dye-loading in the electrodes (in fact there was a reduction in the number of dye molecules), but due to a strong role played by the CNTs in enhancing the conductivity of the TiO_2 electrode. With the high electron mobility [46], the CNTs dispersed into the TiO_2 matrix facilitate faster transport of photoexcited electrons (from the dye) across the TiO_2 network and collection at the electrode surface (a schematic of the processes is shown in Fig. 10) [10,22], thereby increasing the photocurrent density and minimizing the recombination at grain boundaries. This is further reflected in the IPCE spectra shown in Fig. 9B. From the IPCE traces, we can see that for the DSC with the 0.2 wt% CNTs, the peak of the IPCE was enhanced from 44% to 57% corresponding to an increase of ~30%. The most important factors contributing to the IPCE are the light harvesting efficiency, and charge separation and collection yields [47,48]. The contribution due to the first parameter is negligible because of the nearly similar dye-loadings in the TiO_2 and TiO_2–CNT samples. As the normalized IPCE spectra retain similar shape, the wavelength-independent charge separation can partially account for the IPCE maxima difference, probably due to dissimilar yields of electron injection. Further, the equilibration of electrons between TiO_2 and CNTs (the Fermi level equilibration) results in a transfer of a fraction of electrons from TiO_2 to the CNTs and this stabilizes the photoinjected electrons (charge separation) thus minimizing the rate of excitons recombination [22]. Additionally, as faster electron transport across the TiO_2 network and minimization of back electron transfer are known to influence the IPCE results; it can be concluded that the 30% enhancement of the IPCE in the present case comes as a direct consequence of all the above contributing factors [23].

Table 1
Photovoltaic parameters for CNTs-incorporated TiO_2 electrodes in DSCs.

CNT (wt%)	J_{sc} (mA/cm^2)	V_{oc} (V)	Fill factor	Efficiency (%)
0	9.40 ± 0.15	0.815 ± 0.015	0.60 ± 0.02	4.63 ± 0.25
0.1	10.45 ± 0.1	0.820 ± 0.01	0.62 ± 0.02	5.34 ± 0.25
0.2	11.98 ± 0.1	0.820 ± 0.01	0.62 ± 0.02	6.12 ± 0.25
0.3	11.22 ± 0.1	0.798 ± 0.01	0.61 ± 0.02	5.48 ± 0.25

However, when the CNTs concentration was further increased to 0.3 wt%, the efficiency of the DSCs started to decrease. The energy conversion efficiency decreased from 6.12% to 5.48%, with the J_{sc} decreased from 11.98 mA/cm^2 to 11.22 mA/cm^2, the V_{oc} decreased from 0.82 V to 0.798 V, and the FF decreased from 0.62 to 0.61. This trend was seen with still further increase in the CNT concentrations in TiO_2. This could be because of the following reasons: (a) the conduction band of CNT (−4.5 eV) is more negative than the conduction band of TiO_2 (−4.2 eV) [49] and increase in the CNT concentration in the composite would cause a shift in the apparent Fermi level of the composite to more positive potentials due to charge equilibration between the systems (Fig. 10) [22], which induces a slightly decrease of the V_{oc} from 0.82 V to 0.798 V in the present case, (b) high concentration of CNTs in the electrodes makes it less optically transparent and hence the light harvesting of N3 dye would be challenged, and (c) a reduction in the effective dye-loading on the TiO_2 electrode [23] by the excess CNTs (this was verified in the present case with dye-desorption measurements in Fig. 9A).

A comparison of our results with the literature attempts in similar directions is outlined below. Lee et al. [20,21] and Yen et al. [25] synthesized TiO_2-coated CNTs and TiO_2–CNT, respectively, through sol–gel and sonication-assisted mixing routes. The V_{oc} observed in the composites (~0.63 V, 0.78 V and 0.73 V, respectively) and the best efficiencies (~5% and ~4.6%, respectively) reported were lower than that in the present case (0.82 V and 6.12%, respectively). Muduli et al. [23] reported the synthesis of TiO_2–CNT composites by hydrothermal route and observed an efficiency enhancement of ~50% compared to P-25 (the J_{sc} before and after incorporating CNTs was 14.9 mA/cm^2 and 21.9 mA/cm^2, respectively). However, the V_{oc} and FF reported in the case were much lower (0.7 V and ~0.5, respectively) than that in the present case. The V_{oc} observed in the present case was higher than that in yet another literature attempt where the CNTs were mixed with TiO_2 via sonication [24]. This is consistent with our general experimental observation that the DSCs with the rice grain-shaped TiO_2 consistently showed higher V_{oc} than the nanoparticle systems [35]. When the nanostructures were directly electrospun on FTO plates (however, this is very challenging as most of the electrodes crack during sintering owing to volume shrinkage associated with the polymer evaporation), we have noted a record V_{oc} of 0.96 V as the fabrication of photoanode by this manner ensures excellent morphology retainment, connectivity and natural compact packing of the nanostructures [34,39,40]. The 1-D TiO_2–CNT composite in the present case is single crystalline and can ensure better connectivity between the nanostructures which thus facilitate a smooth charge transport through the TiO_2 network.

3.3. Electrochemical impedance spectra (EIS)

To get an insight into the better charge transport and collection in the DSCs with the TiO_2–CNT composite, EIS measurements were performed. EIS of different of electrodes were measured in the frequency range of 30 kHz–0.05 Hz under dark condition. In a

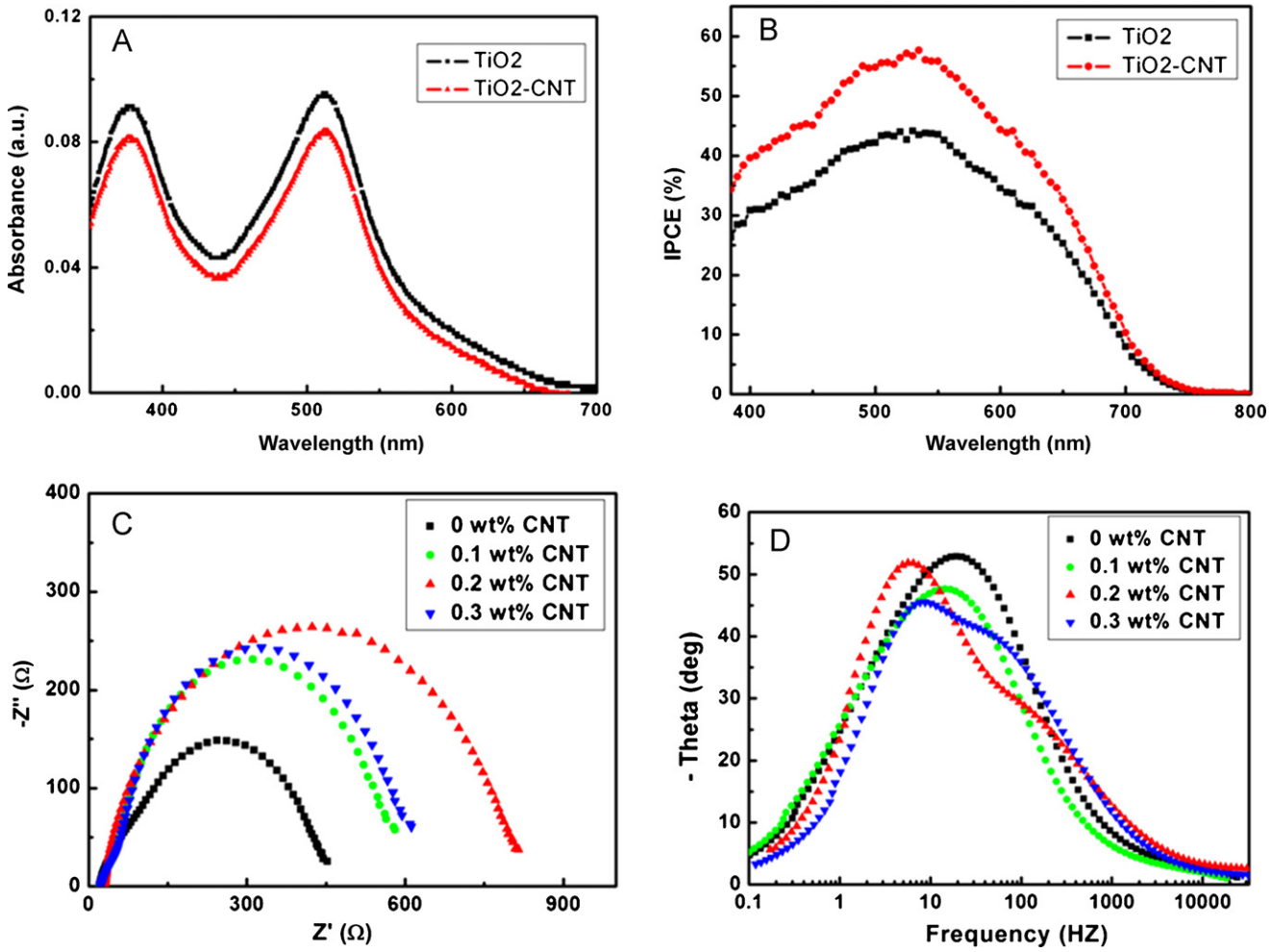

Fig. 9. UV–vis spectra of dye detached from TiO_2 and TiO_2–CNT electrodes (A); IPCE of electrodes of TiO_2 ad TiO_2–CNT (0.2 wt%) (B); Nyquist plot of all the electrodes (C); and Bode phase plots of all the electrodes (D).

typical Nyquist plot, there are three semicircles; the ones at low and high frequency regions represent electrochemical reaction at the Pt counter electrode and the diffusion process of I^-/I_3^- ions in the electrolyte, respectively. The low frequency semicircle was absent in the present case (even at low bias voltages) due to the large charge transport resistance shown by the TiO_2. The semicircle at the intermediate (middle) frequency corresponds to the charge recombination resistance at the TiO_2/dye/electrolyte interface which is a most important parameter affecting the efficiency of DSC devices [50–52]. The larger the charge recombination resistance, the lower the charge recombination rate will be. As shown in the spectra in the Fig. 9C, the semicircle at the intermediate frequency increased as the CNTs concentration was increased from 0 to 0.2 wt%. This indicated a higher resistance for recombination

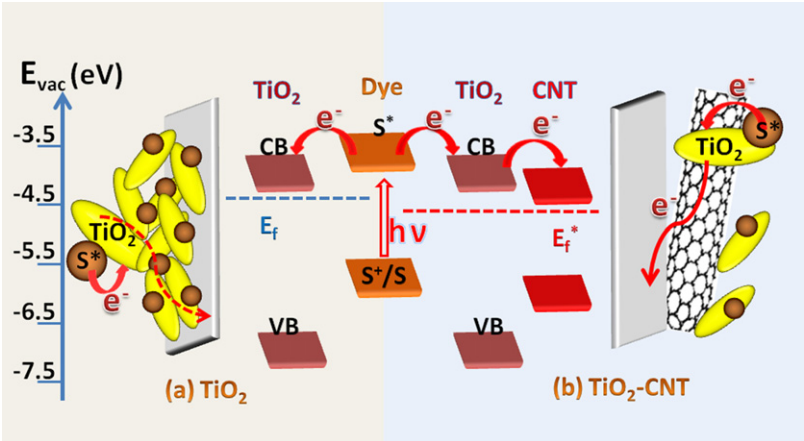

Fig. 10. Energy band diagram illustrating the charge injection and charge transport from excited sensitizer into TiO_2 and to the conductive glass without (a) and with (b) CNT network, and the equilibration of the Fermi levels (from E_f to E_f^*).

which implies that the charge recombination between the injected electrons and the electron acceptors in the redox electrolyte was remarkably retarded [53]. This is in agreement with the enhanced photocurrent density seen in the *I–V* characteristics which is further reflected in the Bode phase plots shown in Fig. 9D. The characteristic frequency peaks shifted to lower frequencies with the increase in CNTs concentration from 0 to 0.2 wt% and then shifted back to higher frequency when the CNT concentration was increased to 0.3 wt%. Through a correlation of frequency maximum (f_{mid}) to the electron lifetime (τ_e) of photoexcited electrons in TiO_2 films [54] by using the equation, $\tau_e = 1/(2\pi f_{mid})$, we can see that compared to the electron lifetime of 7.6 ms in TiO_2 (f_{mid} = 20.8 Hz), the 0.2 wt% TiO_2–CNT composite showed a higher electron lifetime of 27 ms (f_{mid} = 5.9 Hz). This implied that the electrons live longer in the TiO_2–CNT network [22], further implying the reduced recombinations. It must also be noted that in the Bode phase plots of TiO_2–CNTs (with 0.2 and 0.3 wt% CNTs), an additional peak also emerges at higher frequency and the intensity of which increases with increase in the amount of CNTs in TiO_2 (evident in the case of the 0.3 wt% CNTs). Though the exact reason for the origin of the second peak is not clear to us at the moment, however, the trend is an indication of the shift of the peak maximum to higher frequencies when the CNT content in TiO_2 is large enough. This trend may correlate well with the systematic changes in photovoltaic parameters with increase in CNTs observed above.

4. Conclusions

The rice-grain shaped TiO_2–CNT nanocomposites with high surface area and single crystallinity (for TiO_2) were fabricated by electrospinning. The nanostructures were characterized by spectroscopy and microscopy. DSCs fabricated using the materials having systematically varied CNT concentrations in TiO_2 matrix showed that the photovoltaic parameters increased with increases in CNT concentrations, reach a maximum and then decreased. It was found that the optimum concentration of CNTs in TiO_2 matrix for best DSC performance was 0.2 wt%, which produced an efficiency enhancement of 32% when compared to bare TiO_2. The beneficial effect of CNTs in the charge transport, collection and overall improvement of efficiency has been confirmed by *I–V*, IPCE and EIS investigations. We believe that the simple and cost-effective fabrication of the novel composite would find a host of applications in other areas as well namely photocatalysis, self cleaning membranes, photonic crystals, etc.

Acknowledgments

Z.P, Y.S and N.K.E thank National University of Singapore for Ph.D fellowships. A.S.N and S.R thank National Research Foundation and M3TC (Economic Development Board), Singapore for financial support (Grant numbers: NRF 2007 EWT-CERP 01-0531, NRF-CRP4-2008-03 and R-261-501-018-414).

Appendix A. Supplementary data

Supplementary data associated with this article can be found, in the online version, at doi:10.1016/j.jphotochem.2012.01.002.

References

[1] B. O'Regan, M. Grätzel, A low-cost, high-efficiency solar cell based on dye-sensitized colloidal TiO_2 films, Nature 353 (1991) 737–740.
[2] M. Grätzel, Conversion of sunlight to electric power by nanocrystalline dye-sensitized solar cells, J. Photochem. Photobiol. A: Chem. 164 (2004) 3–14.
[3] M. Song, Y. Ahn, S. Jo, D. Kim, J. Ahn, TiO_2 single-crystalline nanorod electrode for quasi-solid-state dye-sensitized solar cells, Appl. Phys. Lett. 87 (2005) 113113.
[4] R. Mane, W. Lee, H. Pathan, S. Han, Nanocrystalline TiO_2/ZnO thin films: fabrication and application to dye-sensitized solar cells, J. Phys. Chem. B 109 (2005) 24254.
[5] S. Hore, C. Vetter, R. Kern, H. Smit, A. Hinsch, Influence of scattering layers on efficiency of dye-sensitized solar cells, Sol. Energy Mater. Sol. Cells 90 (2006) 1176–1188.
[6] B. O'Regan, J. Durrant, P. Sommeling, N. Bakker, Influence of the $TiCl_4$ treatment on nanocrystalline TiO_2 films in dye-sensitized solar cells. 2. Charge density, band edge shifts, and quantification of recombination losses at short circuit, J. Phys. Chem. C 111 (2007) 14001–14010.
[7] R. Koehorst, G. Boschloo, T. Savenije, A. Goossens, T. Schaafsma, Spectral sensitization of TiO_2 substrates by monolayers of porphyrin heterodimers, J. Phys. Chem. B 104 (2000) 2371–2377.
[8] T. Hoshikawa, T. Ikebe, M. Yamada, R. Kikuchi, K. Eguchi, Preparation of silica-modified TiO_2 and application to dye-sensitized solar cells, J. Photochem. Photobiol. A: Chem. 184 (2006) 78–85.
[9] T. Ma, M. Akiyama, E. Abe, I. Imai, High-efficiency dye-sensitized solar cell based on a nitrogen-doped nanostructured titania electrode, Nano Lett. 5 (2005) 2543–2547.
[10] A. Kongkanand, R. Domínguez, P.V. Kamat, Single wall carbon nanotube scaffolds for photoelectrochemical solar cells. Capture and transport of photogenerated electrons, Nano Lett. 7 (2007) 676–680.
[11] Z. Tian, J. Voigt, J. Liu, B. Mckenzie, H. Xu, Large oriented arrays and continuous films of TiO_2-based nanotubes, J. Am. Chem. Soc. 125 (2003) 12384–12385.
[12] B. Tan, Y. Wu, Dye-sensitized solar cells based on anatase TiO_2 nanoparticle/nanowire composites, J. Phys. Chem. B 110 (2006) 15932–15938.
[13] X. Feng, K. Shankar, O. Varghese, M. Paulose, T. Latempa, C. Grimes, Vertically aligned single crystal TiO_2 nanowire arrays grown directly on transparent conducting oxide coated glass: synthesis details and applications, Nano Lett. 8 (2008) 3781–3786.
[14] J. Jennings, A. Ghicov, L. Peter, P. Schmuki, A. Walker, Dye-sensitized solar cells based on oriented TiO_2 nanotube arrays: transport, trapping, and transfer of electrons, J. Am. Chem. Soc. 130 (2008) 13364–13372.
[15] R.P. Lynch, A. Ghicov, P. Schmuki, A photo-electrochemical investigation of self-organized TiO_2 nanotubes, J. Electrochem. Soc. 157 (2010) G76.
[16] S. Pavasupree, S. Ngamsinlapasathian, M. Nakajima, Y. Suzuki, S. Yoshikawa, Synthesis, characterization, photocatalytic activity and dye-sensitized solar cell performance of nanorods/nanoparticles TiO_2 with mesoporous structure, J. Photochem. Photobiol A: Chem. 184 (2006) 163–169.
[17] S. Yang, A.S. Nair, R. Jose, S. Ramakrishna, Electrospun TiO_2 nanorods assembly sensitized by CdS quantum dots: a low-cost photovoltaic material, Energy Environ. Sci. 3 (2010) 2010–2014.
[18] I. Flores, J. Freitas, C. Longo, M. Paoli, H. Winnischofer, A. Nogueira, Dye-sensitized solar cells based on TiO_2 nanotubes and a solid-state electrolyte, J. Photochem. Photobiol. A: Chem. 189 (2007) 153–160.
[19] K. Zhu, N. Neale, A. Miedaner, A. Frank, Enhanced charge-collection efficiencies and light scattering in dye-sensitized solar cells using oriented TiO_2 nanotubes arrays, Nano Lett. 7 (2007) 69–74.
[20] K.M. Lee, C.W. Hu, H.W. Chen, K.C. Ho, Incorporating carbon nanotube in a low-temperature fabrication process for dye-sensitized TiO_2 solar cells, Sol. Energy Mater. Sol. Cells 92 (2008) 1628–1633.
[21] T.Y. Lee, P.S. Alegaonkar, J.B. Yoo, Fabrication of dye sensitized solar cell using TiO_2 coated carbon nanotubes, Thin Solid Films 515 (2007) 5131–5135.
[22] P. Brown, K. Takechi, P.V. Kamat, Single-walled carbon nanotube scaffolds for dye-sensitized solar cells, J. Phys. Chem. C 112 (2008) 4776–4782.
[23] S. Muduli, W. Lee, V. Dhas, S. Mujawar, M. Dubey, K. Vijayamohanan, S.H. Han, S. Ogale, Enhanced conversion efficiency in dye-sensitized solar cells based on hydrothermally synthesized TiO_2-MWCNT nanocomposites, ACS Appl. Mater. Interfaces 1 (2009) 2030–2035.
[24] T. Sawatsuk, A. Chindaduang, C. Sae-kung, S. Pratontep, G. Tumcharern, Dye-sensitized solar cells based on TiO_2-MWCNTs composite electrodes: performance improvement and their mechanisms, Diamond Relat. Mater. 18 (2009) 524–527.
[25] C.Y. Yen, Y.F. Lin, S.H. Liao, C.C. Weng, C.C. Huang, Y.H. Hsiao, C.C. Ma, M.C. Chang, H. Shao, M.C. Tsai, C.K. Hsieh, C.H. Tsai, F.B. Weng, Preparation and properties of a carbon nanotube-based nanocomposite photoanode for dye-sensitized solar cells, Nanotechnology 19 (2006) 375305.
[26] S. Jang, R. Vittal, K. Kim, Incorporation of functionalized single-wall carbon nanotubes in dye-sensitized TiO_2 solar cells, Langmuir 20 (2004) 9807–9810.
[27] B. Gao, G.Z. Chen, G.L. Puma, Carbon nanotubes/titanium dioxide (CNTs/TiO_2) nanocomposites prepared by conventional and novel surfactant wrapping sol–gel methods exhibiting enhanced photocatalytic activity, Appl. Catal. B 89 (2009) 503–509.
[28] H. Yu, X. Quan, S. Chen, H. Zhao, Y. Zhang, TiO_2-carbon nanotube heterojunction arrays with a controllable thickness of TiO_2 layer and their first application in photocatalysis, J. Photochem. Photobiol. A: Chem. 200 (2008) 301–306.
[29] G.J. Hu, X.F. Meng, X.Y. Feng, Y.F. Ding, S.M. Zhang, M.S. Yang, Anatase TiO_2 nanoparticles/carbon nanotubes nanofibers: preparation, characterization and photocatalytic properties, J. Mater. Sci. 42 (2007) 7162–7170.
[30] S. Kedem, J. Schmidt, Y. Paz, Y. Cohen, Composite polymer nanofibers with carbon nanotubes and titanium dioxide particles, Langmuir 21 (2005) 5600–5604.
[31] S. Aryal, C.K. Kim, K.W. Kim, M.S. Khil, H.Y. Kim, Multi-walled carbon nanotubes/TiO_2 composite nanofiber by electrospinning, Mater. Sci. Eng. C 28 (2008) 75–79.
[32] W.G. Fan, L. Gao, J. Sun, Anatase TiO_2-coated multi-wall carbon nanotubes with the vapor phase method, J. Am. Ceram. Soc. 89 (2006) 731–733.

[33] A. Jitianu, T. Cacciaguerra, R. Benoit, S. Delpeux, F. Beguin, S. Bonnamy, Synthesis and characterization of carbon nanotubes—TiO_2 nanocomposites, Carbon 42 (2004) 1147–1151.
[34] A.S. Nair, S.Y. Yang, P.N. Zhu, S. Ramakrishna, Rice grain-shaped TiO_2 mesostructures by electrospinning for dye-sensitized solar cells, Chem. Commun. 46 (2010) 7421–7423.
[35] S.Y. Yang, P.N. Zhu, A.S. Nair, S. Ramakrishana, Rice grain-shaped TiO_2 mesostructures—synthesis, characterization and applications in dye-sensitized solar cells and photocatalysis, J. Mater. Chem. 21 (2011) 6541–6548.
[36] P.N. Zhu, A.S. Nair, S.Y. Yang, S. Ramakrishna, TiO_2–MWCNT rice grain-shaped nanocomposites—synthesis; characterization and photocatalysis, Mater. Res. Bull. 46 (2010) 588–595.
[37] P.N. Zhu, Y.Z. Wu, M.V. Reddy, A.S. Nair, S.B.V.R. Chowdari, S. Ramakrishna, Long term cycling studies of electrospun TiO_2 nanostructures and their composites with MWCNTs for rechargeable Li-ion batteries, RSC Adv. 2 (2012) 531–537.
[38] A.S. Nair, R. Jose, S.Y. Yang, S. Ramakrishna, A simple recipe for an efficient TiO_2 nanofiber-based dye-sensitized solar cell, J. Colloid Interface Sci. 1 (2011) 39–45.
[39] S.R. Williams, A.P. Philipse, Random packings of spheres and spherocylinders simulated by mechanical contraction, Phys. Rev. E: Stat. Nonlinear Soft Matter Phys. 67 (2003) 051301.
[40] A. Wouterse, S. Luding, A.P. Philipse, On contact numbers in random rod packings, Granul. Matter. 11 (2009) 169–177.
[41] A. Peigney, C. Laurent, E. Flahaut, R.R. Bacsa, A. Rousset, Specific surface area of carbon nanotubes and bundles of carbon nanotubes, Carbon 39 (2001) 507–514.
[42] Q. Liang, L.Z. Gao, Q. Li, S.H. Tang, B.C. Liu, Z.L. Yu, Carbon nanotube growth on Ni-particles prepared in situ by reduction of La_2NiO_4, Carbon 39 (2001) 897–903.
[43] L. Chen, Y. Ho, W. Guo, C. Huang, T. Pan, Enhanced visible light-induced photoelectrocatalytic degradation of phenol by carbon nanotube-doped TiO_2 electrodes, Electrochim. Acta 54 (2009) 3884–3891.
[44] G. An, W. Ma, Z. Sun, Z. Liu, B. Han, S. Miao, Z. Miao, K. Ding, Preparation of titania/carbon nanotube composites using supercritical ethanol and their photocatalytic activity for phenol degradation under visible light irradiation, Carbon 45 (2007) 1795–1801.
[45] Q. Akhavan, R. Azimirad, S. Safa, M. Larijani, Visible light photo-induced antibacterial activity of CNT–doped TiO_2 thin films with various CNT contents, J. Mater. Chem. 20 (2010) 7386–7392.
[46] M. Grado-Caffaro, Theoretical evaluation of electron mobility in multi-walled carbon nanotubes, Opt. Int. J. Light Electron Opt. 115 (2004) 45–46.
[47] J. Bisquert, D. Cahen, G. Hodes, S. Ruehle, A. Zaban, Physical chemical principles of photovoltaic conversion with nanoparticulate, mesoporous dye-sensitized solar cells, J. Phys. Chem. B 108 (2004) 8106–8118.
[48] M. Grätzel, Solar energy conversion by dye-sensitized photovoltaic cells, Inorg. Chem. 44 (2005) 6841–6851.
[49] M. Grätzel, Photoelectrochemical cells, Nature 414 (2001) 338–344.
[50] F. Santiago, J. Bisquert, G. Belmonte, G. Boschloo, A. Hagfeldt, Influence of electrolyte in transport and recombination in dye-sensitized solar cells studied by impedance spectroscopy, Sol. Energy Mater. Sol. Cells 87 (2005) 117–131.
[51] J. Bisquert, Theory of the impedance of electron diffusion and recombination in a thin layer, J. Phys. Chem. B 106 (2002) 325–333.
[52] Q. Wang, J. Moser, M. Grätzel, Electrochemical impedance spectroscopic analysis of dye-sensitized solar cells, J. Phys. Chem. B 109 (2005) 14945–14953.
[53] N. Yang, J. Zhai, D. Wang, Y. Chen, L. Jiang, Two-dimensional graphene bridges enhanced photoinduced charge transport in dye-sensitized solar cells, ACS Nano 4 (2010) 887–894.
[54] R. Kern, R. Sastrawan, J. Ferber, R. Stangl, J. Luther, Modeling and interpretation of electrical impedance spectra of dye solar cells operated under open-circuit conditions, Electrochim. Acta 47 (2002) 4213–4225.